Applied Catalysis A, General 567 (2018) 36–44

Contents lists available at ScienceDirect

Applied Catalysis A, General

journal homepage: www.elsevier.com/locate/apcata

Bimetallic catalysts supported on novel spherical $MgAl_2O_4$-coated supports for dehydrogenation processes

S.R. de Miguel, I.M.J. Vilella, P. Zgolicz, S.A. Bocanegra*

Instituto de Investigaciones en Catálisis y Petroquímica "Ing. José M. Parera" (INCAPE), Facultad de Ingeniería Química (Universidad Nacional del Litoral)-CONICET, Colectora, Ruta 168 Km 0 - (3000), Santa Fe, Argentina

ARTICLE INFO

Keywords:
Structured spherical catalysts
Dehydrogenation
Butenes
Bimetallic catalysts

ABSTRACT

Novel Pt and PtSn catalysts were developed from structured supports of α-Al_2O_3 spheres coated with $MgAl_2O_4$ by two methods: advanced Bohemite-nitrate with purification (BNAP) and citrate-nitrate with two layers (CN2). Both structured supports showed a thin porous layer of $MgAl_2O_4$ with a high specific surface area of around 130 m^2 g^{-1}. A stable and uniform $MgAl_2O_4$ layer on the spherical nuclei was achieved by both synthesized coating methods. Therefore, a good interaction with the metals which leads to high metallic dispersions was obtained. These catalysts were used in the production of butenes by n-butane dehydrogenation reaction. The bimetallic catalysts showed both high values of n-butane conversion (25–30 %) and selectivity to butenes (89–95 %). The PtSn catalyst supported on spheres coated by CN2 method displayed high values of yield to butenes (about 30%), which are higher than those of a catalyst used in the industry.

1. Introduction

The development of more efficient catalysts for mass and heat transfer and with high yields to the desired products is a constant challenge in the petrochemical industry. In this sense, fast reactions carried out at high temperatures, such as the direct dehydrogenation of alkanes, need catalysts that avoid heat and mass-transfer limitations and minimize undesirable reactions like cracking of alkanes, alkenes polymerization and coke formation. The most used catalysts in the direct dehydrogenation of alkanes are the metallic ones (Pt or Pd with promoters) supported on Al_2O_3, Al_2O_3 with alkaline or earth-alkaline metals, Al_2O_3 with lanthanides, SiO_2, hydrotalcites or $MgAl_2O_4$ spinel [1–6]. With respect to the metals, the most used in dehydrogenation reaction is Pt with promoters as Sn, In, Ga, Ge, etc. [2–4,7–10]. With regards to the effect of the support on the catalytic properties, it has been largely studied that both the low acidity and a good interaction with the metallic phase, are necessary to improve the catalytic behavior. Pt catalysts (with Sn and In promoters) supported on magnesium spinel showed a very good catalytic performance in the direct dehydrogenation of alkanes to the corresponding monoalkenes [3,8,11–13].

The development of structured catalysts from new materials and techniques is an area that has acquired importance in recent years. The advance of coating techniques has allowed the deposition of the active catalytic components in a thin layer, improving mass and heat transfer coefficients. The coating methods for catalyst synthesis are dip-coating, blowing-coating, sol-gel, electrodeposition, chemical vapor deposition. The selection of the method will depend mainly on the substrate and on the coating material [14–21].

In this study, structured supports consisting on compact spheres of α-Al_2O_3 covered with a thin and porous layer of magnesium spinel obtained by two methods were synthesized. These materials were used as supports for PtSn catalysts in the n-butane dehydrogenation reaction for butenes production. The proposed coating methods are based on the dip-coating technique but with novel changes developed in this study. The originality of this work is the coating on a spherical substrate. In this sense, there is a lot of bibliography about coating of metallic oxides in slabs, tubes, plates and foams, but only very few studies based on coating in a spherical geometry [21–23] and coating with magnesium spinel [22,24–26]. It should be mentioned that most of these studies use the magnesium spinel as a protection ceramic material and not as a structured catalyst.

2. Experimental

2.1. Synthesis of structured supports

The starting materials were compact spheres (φ = 2 mm) of commercial α-Al_2O_3 (Sg = 4.7 m^2 g^{-1}) provided by SASOL company.

* Corresponding author.
E-mail address: sbocane@fiq.unl.edu.ar (S.A. Bocanegra).

https://doi.org/10.1016/j.apcata.2018.09.005
Received 2 July 2018; Received in revised form 23 August 2018; Accepted 10 September 2018
Available online 18 September 2018
0926-860X/

In order to develop roughness on the spheres surface to improve the adhesion of the coating material, they were pretreated with hydrochloric acid solution (1 M).

2.2. Bohemite-nitrate advanced with purification (BNAP) coating method

For this method, commercial bohemite, AlO(OH) (Disperal P2), provided by SASOL company, and $Mg(NO_3)_2$. 6 H_2O (Sigma Aldrich, purity 99.5%) were used.

Three suspensions of AlO(OH) with nitric acid were prepared: 5 wt %, 10 wt % and 15 wt %. The spheres were placed in a basket in continuous rotation and submerged in bohemite gel 5 wt % and then dried in hot air flow. This process was repeated with the gels of 10 wt % and 15 wt %. Finally, the spheres were dried in furnace at 110 °C for 24 h.

The spheres covered with AlO(OH) were impregnated with solution of $Mg(NO_3)_2.6H_2O$ (0.5 M) and then they were dried in furnace and finally calcined in air flow at 850 °C to form the magnesium spinel ($MgAl_2O_4$).

The XRD analysis results of the coating layer material showed the diffraction peaks corresponding both to $MgAl_2O_4$ and MgO (product of incomplete reaction). In order to purify the magnesium spinel the coated spheres were submitted to a treatment with solution of $(NH_4)_2CO_3$ (1 M), as it has been previously studied [27]. More details about the preparation of this structured material can be seen in reference [28].

2.3. Citrate-nitrate with two layers (CN2) coating method

The reagents used at this stage were: $Mg(NO_3)_2$. 6 H_2O (Sigma Aldrich, purity 99.5%), $Al(NO_3)_3.9H_2O$ (Sigma Aldrich, purity 99.5%) and citric acid monohydrate ($C_6H_8O_7.H_2O$) (Sigma-Aldrich, purity 99.5%).

A solution of $Mg(NO_3)_2$. 6 H_2O, $Al(NO_3)_3.9H_2O$ and $C_6H_8O_7.H_2O$ with molar ratio [Al/Mg] = 2, and [citric acid/nitrate ions] molar ratio equal to 0.5 was prepared. The spheres were put in a beaker together with the solution and maintained in soft stirring. The solution was heated up to the boiling point and kept under boiling during 30 min for the gel to be formed. Then, the gel and the spheres were dried in vacuum during 24 h at low temperature (75–100 °C). Later, the dried gel and the spheres were calcined in N_2 flow at 500 °C, in nitrogen and oxygen flow (5 v/v % O_2-N_2) at 700 °C and, finally in air flow at 800 °C to form the magnesium spinel ($MgAl_2O_4$). The whole process was repeated once more so as to increase the thickness of the layer on the substrate. More details about the preparation of this structured material can be seen in reference [29].

2.4. Characterization of structured supports

The supports obtained by BNAP and CN2 methods were characterized by SEM to verify the formation of a uniform thin layer on the spheres. X-ray diffraction (XRD) analyses were carried out on the coating material to be certain about the $MgAl_2O_4$ spinel formation. Textural properties, specific surface area and pore volume, were determined using BET adsorption isotherm.

SEM microphotographs were made using a JSM-35C equipment, JEOL model, with a SemAfore digital image acquisition system. The experiments were performed as images of secondary electrons using an acceleration voltage of 20 kV. The spheres and half spheres (obtained by cutting with an scalpel) were adhered in the surface of a glass microscope slide. Then the samples were covered with a thin layer of gold by sputtering to give them conductivity before the observations. The powder residues in the bed of the quartz reactor after the calcination step of the coated spheres (by both methods: BNAP and CN2), were characterized by XRD to confirm the formation of $MgAl_2O_4$ spinel in the layer. These analyses were carried out in a Shimadzu model XD3A equipment with CuK_α radiation (λ = 1542 Å). The parameters of the analysis were: Cu target, voltage: 30 kV, current: 30 mA, sampling rate: $1^\circ\,min^{-1}$, predetermined time: 1.0 s.

The specific surface area and pore volume of the samples were obtained by N_2 adsorption at −196 °C using Micromeritics equipment, ASAP 2020 model.

2.5. Catalysts preparation

Pt monometallic catalysts were prepared by impregnation of coated spheres obtained by BNAP and CN2 methods with solution of $H_2Cl_2Pt_6$ (chloroplatinic acid). The coated spheres were placed in a beaker and then covered with a given volume of chloroplatinic acid solution as to obtain a Pt content of 0.3 wt%. The [impregnation volume/spheres weight] ratio was $1.4\,mL\,g^{-1}$, and the impregnation time was 6 h at room temperature. Then, the samples were dried in furnace at 110 °C for 12 h and subsequently calcined at 500 °C in air flow for 3 h. The catalysts obtained were named: Pt/E-Mg-BNAP and Pt/E-Mg-CN2.

Bimetallic PtSn catalysts were obtained from Pt/E-Mg-BNAP and Pt/E-Mg-CN2 catalysts before the calcination step. The dried monometallic catalysts were impregnated with $SnCl_2$ solution (with HCl) using a [impregnation volume/spheres weight] ratio of $1.4\,mL\,g^{-1}$ and a concentration to achieve 0.3 wt % of Sn. The impregnation time was 6 h at room temperature. Then, the samples were dried in furnace at 110 °C for 12 h and subsequently calcined at 500 °C in air flow for 3 h. The catalysts obtained were named: PtSn/E-Mg-BNAP and PtSn/E-Mg-CN2. The Pt and Sn concentrations in the catalysts were determined by Inductively Coupled Argon Plasma Emission Spectrometry (ICP-AES), and they ranged between 95 and 100% of the nominal values.

2.6. Catalysts characterization

Mono and bimetallic catalysts were characterized by H_2 chemisorption measurements, Temperature-programmed Reduction (TPR), X-ray Photoelectron Spectroscopy (XPS), Transmission Electron Microscopy (TEM) and test reactions of metallic phase: cyclohexane dehydrogenation (CHD) and cyclopentane hydrogenolisis (CPH).

H_2 chemisorption measurements were carried out in a static volumetric equipment. The sample was outgassed for 30 min at room temperature and high vacuum (10^{-5} mmHg) followed by a reduction in H_2 flow at 500 °C for 2 h and outgassed for 2 more hours at 500 °C at high vacuum. Then, the sample was cooled down at room temperature and H_2 dosage was made. The adsorption isotherms were linear between 25 and 150 mm Hg of hydrogen pressure. The chemisorbed hydrogen monolayer was determined from the extrapolation of the isotherm to pressure zero.

TPR experiments were carried out in flow reactor using a reductive gaseous mixture of H_2 and N_2 (5 v/v % H_2 - N_2) with a flow rate of $9\,mL\,min^{-1}$. The samples were heated from room temperature up to 650 °C at a heating rate of $6\,^\circ C min^{-1}$. Previously the catalysts were calcined “in situ” at 500 °C during 3 h in air flow.

XPS measurements were carried out in a VG-Microtech Multilab Spectrometer. The energy power of the instrument was 50 eV (radiation MgKα, $h\nu$ = 1253.6 eV). The vacuum in the analysis chamber was 4.10^{-10} T. The samples were previously reduced “in situ” with H_2 for 2 h at 500 °C. Binding energies (BE) were referred to the C1s signal at 284.9 eV. The experimental data were fitted with Lorentzian-Gaussian curves to estimate the peak areas using CasaXPS software.

TEM measurements were performed using a JEOL 100CX Microscope. The instrument was operated with an acceleration voltage of 100 KV, and magnification ranges of 80,000x and 100,000×. The samples for these experiments were obtained by the following process: the reduced catalysts were carefully scrapped using an scalpel to withdraw the layer and then the powder was ground and suspended in ethanol. A drop of this suspension was placed on a carbon copper grid. After the alcohol evaporation, the samples were introduced into the microscope column. For each catalyst, a very significant number of Pt

particles (~100) was observed and the distribution curves of particle sizes were done. The formula to calculate the mean metallic particle diameter ($\overline{D}$) was:

$\overline{D} = \sum_i ni.\ di / \sum_i ni$, where ni is the number of particles of diameter di.

The reaction tests of the metallic phase, cyclohexane dehydrogenation (CHD) and cyclopentane hydrogenolysis (CPH), were performed in a differential flow reactor with a volumetric flow of 6 $cm^3\,h^{-1}$. Before the reaction, the catalysts were reduced "in situ" in hydrogen flow for 2 h. The products were analyzed by gas chromatography. The CPH (metallic structure-sensitive reaction [30]) was carried out at 500 °C using a [H_2/CP] molar ratio of 22. The CHD (metallic structure-insensitive reaction [30]) was carried out at 300 °C and the [H_2/CH] molar ratio in the feed was 26. A linear regression with reaction rates at three temperatures (290 °C, 300 °C and 310 °C) in Arrhenius graph was made to measure the activation energy.

2.7. Catalytic experiments in n-butane dehydrogenation reaction

The reaction was carried out in a quartz flow reactor at 530 °C for 2 h. The weight of the catalyst was 0.2 g and the reactive n-butane was fed together with hydrogen gas in H_2/n-C_4H_{10} molar ratio = 1.25 with a total flow of 18 mL min^{-1}. The gases used had a purity > 99,95 %. Before the reaction, the catalyst was reduced "in situ" in hydrogen flow for 3 h at 500 °C. The reaction products were analyzed in a gas chromatography equipped with a FID detector and a packed chromatographic column (20% BMEA on Chromosorb P-AW 60/80). This analytical instrument allows the separation and quantification of methane, ethane, ethylene, propane, propylene, n-butane, 1-butene, cis-2-butene, trans-2-butene and 1,3-butadiene. The contribution of homogeneous reaction was negligible in these experiments.

3. Results and discussion

The specific surface area of α-Al_2O_3 spheres pretreated with HCl solution was 5.0 $m^2\,g^{-1}$. After the application of BNAP and CN2 coating methods, the covered spheres showed a specific surface area of 22.3 $m^2\,g^{-1}$ and 11.7 $m^2\,g^{-1}$, respectively. In both cases, an important increase in the specific surface area was observed. Coating with BNAP and CN2 methods increases the spheres weight in 16% and 9.4%, respectively. Taking into account the weights and the specific surfaces of the spheres prior and after coating, the specific surface area of the layer was estimated in 139.3 $m^2\,g^{-1}$ for the BNAP method and 124.5 $m^2\,g^{-1}$ for the CN2 one.

SEM microphotographs of coated spheres are shown in Fig. 1 (BNAP method) and Fig. 2 (CN2 method). Fig. 1(a) shows a thin uniform layer that covered the sphere with a thickness of about 30 μm, such as displayed in a cut of the sphere in Fig. 1(b). After the purification process (see experimental section), the layer on the sphere shows a slight peeling (Fig. 1(c)). The cut of the sphere in Fig. 1(d) shows a layer of about 13 μm of thickness. Fig. 2(a) displays a covered sphere of uniform aspect. The cuts of spheres in Fig. 2(b) and (c) shows that the layer on coated spheres is very rough and porous. The thickness of the layer is about 5 μm.

The results of X-ray diffraction analysis of the layer materials obtained by BNAP and CN2 methods are shown in Fig. 3(a) and (b), respectively. In Fig. 3(a), the diffraction peaks corresponding to magnesium spinel and besides, traces of MgO can be observed. In order to remove this impurity, the material was submitted to a purification process using ammonium carbonate solution (see experimental section). It was not possible to carry out the analysis by X-ray diffraction of the layer deposited on the spheres after the purification treatment because when the layer of the spheres were scrapped, small amounts of α-Al_2O_3 were removed from them. This material has very intense diffraction peaks that overlap with those of $MgAl_2O_4$. The material of the layer obtained by CN2 method only showed the diffraction peaks of magnesium spinel (Fig. 3(b)).

The uniform coating layer of an adequate thickness was achieved by applying both methods. The preparation methods influenced the textural properties and the chemical purity of the layer deposited on the spheres.

Pt and PtSn catalysts, synthesized with these materials as supports, were evaluated in n-butane dehydrogenation reaction, and the results are displayed in Figs. 4–6.

The n-butane conversion results (Fig. 4) showed that the monometallic catalysts had different initial conversions, being 30.5% for the Pt/E-Mg-CN2 catalyst and 25.3% for the Pt/E-Mg-BNAP catalyst. Nevertheless, the final conversions were similar, about 21%. Hence, the results indicated a higher initial activity for the Pt/E-Mg-CN2 catalyst than for the Pt/E-Mg-BNAP catalyst, but also a higher deactivation of the first one.

The two bimetallic catalysts showed a different catalytic behavior. The PtSn/E-Mg-BNAP one showed an initial conversion of 25.5% and a final conversion of 22.1%, whereas the PtSn/E-Mg-CN2 one had an initial and final conversion of 31.0% and 30.1% respectively (Fig. 4). The latter displayed higher activity and lower deactivation than the PtSn/E-Mg-BNAP one. In conclusion, the Sn addition to both monometallic catalysts improved the n-butane conversion values and decreased the deactivation along the experiment. However, this change is more evident for the PtSn/E-Mg-CN2 catalyst. In general both bimetallic catalysts were very stable through the reaction time. The deposited carbon contents, analyzed after the reaction, were negligible in all cases.

Fig. 5 displays a very different behavior in the selectivity to butenes between Pt/E-Mg-BNAP and Pt/E-Mg-CN2 samples. The first one showed much higher values of selectivity to butenes than the last one. On the other hand, the bimetallic catalysts displayed similar performances in the selectivity to butenes, with an initial value of 88.6% for PtSn/E-Mg-BNAP one and 93.8% for PtSn/E-Mg-CN2 one and a final value for both samples of about 95%. Hence, the Sn addition increased the selectivities to butenes of both monometallic catalysts, mainly for PtSn/E-Mg-CN2 catalyst. In this case, the final selectivity values increased from 67% to 95%.

Fig. 6 shows a summary of the catalytic behavior of the samples through the initial and final values of the yield to butenes (defined as the product between n-butane conversion and selectivity to butenes). Pt and PtSn catalysts synthesized with BNAP method displayed slight differences in the yield to butenes, whereas bimetallic catalyst prepared by CN2 method showed a notable increase of the initial and final yields to butenes (with values of 29%) respect to the corresponding monometallic catalyst (with values of about 15%). Besides, in Fig. 6 the yields values of a commercial structured multimetallic catalyst (with a support of ceramic spheres and a layer of Al_2O_3) are included for comparison. The PtSn/E-Mg-CN2 catalyst shows a better catalytic performance than the commercial catalyst.

Hydrogen chemisorptions values and results of test reactions (cyclohexane dehydrogenation and cyclopentane hydrogenolysis) of all catalysts are shown in Table 1. For monometallic catalysts, Pt/E-Mg-CN2 catalyst displayed a higher H_2 chemisorption value than Pt/E-Mg-BNAP catalyst, this meaning a higher metallic dispersion for the first catalyst. The metallic dispersion values of both monometallic catalysts are similar or higher than those obtained for Pt catalysts supported on powders of $MgAl_2O_4$ [28]. It must be noticed the very high dispersion of Pt/E-Mg-CN2 catalyst (88%). Besides, in agreement with chemisorption results, the Pt/E-Mg-CN2 catalyst also showed higher initial rate values of CH dehydrogenation (see Table 1). This reaction is a structure-insensitive one, which is carried out on one active site of the catalyst. Hence, these results indicate that this catalyst had more active sites than the Pt/E-Mg-BNAP one. This phenomenon agrees with the results of n-butane reaction, where the Pt/E-Mg-CN2 catalyst also showed higher activity than the Pt/E-Mg-BNAP one throughout the reaction time.

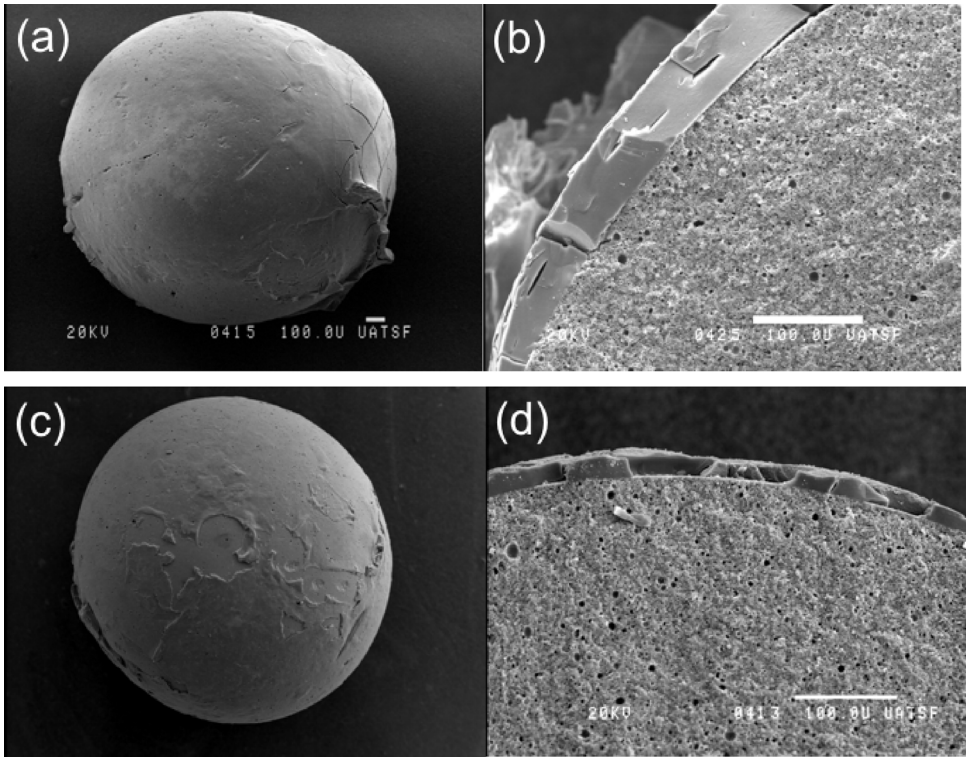

Fig. 1. Microphotographs of spheres and cut of spheres coated with MgAl2O4 by BNAP method: before the purification step (a and b), after the purification step (c and d).

Results of CP hydrogenolysis (a structure-sensitive reaction) for both monometallic catalysts (Table 1) are in agreement with the catalytic behavior in n-butane dehydrogenation. In this sense, the low selectivity to butenes of the Pt/E-Mg-CN2 catalyst would be attributed to its high hydrogenolytic activity (see Table 1).

The Sn addition to monometallic catalysts modifies the metallic phase, decreasing the values of hydrogen chemisorption, initial rates of CH dehydrogenation and initial rates of CP hydrogenolysis. Nevertheless, both bimetallic catalysts showed different behaviors. The PtSn/E-Mg-CN2 catalyst displayed a fall of 7.7 times in the hydrogen

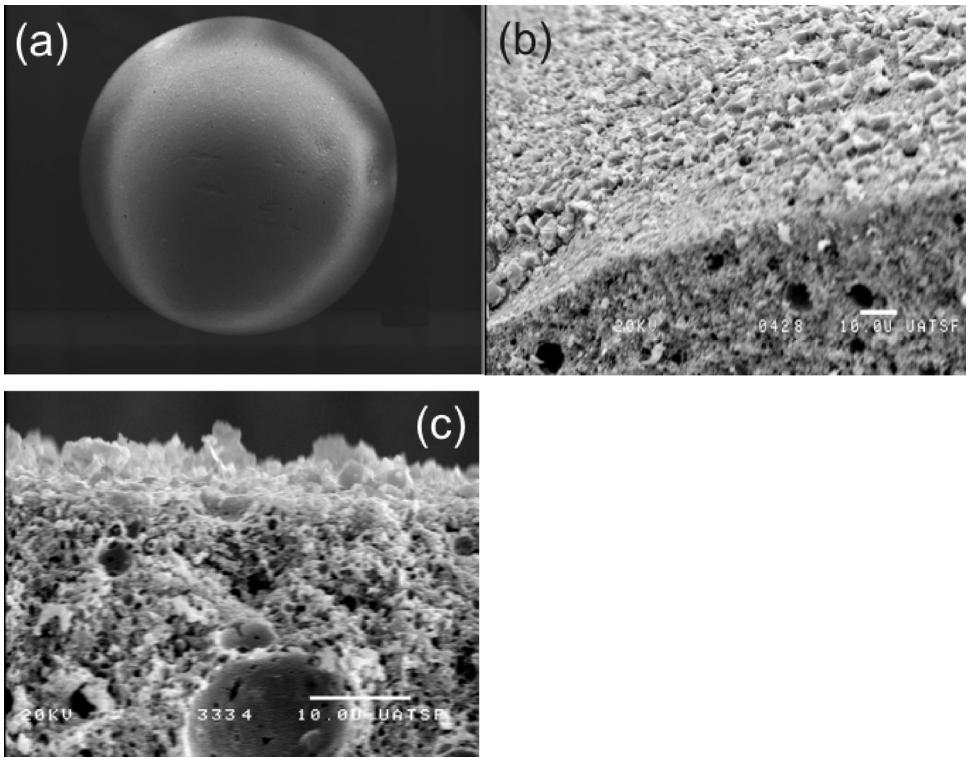

Fig. 2. Microphotographs of spheres and cut of spheres coated with MgAl2O4 by CN2 method: (a), (b) and (c).

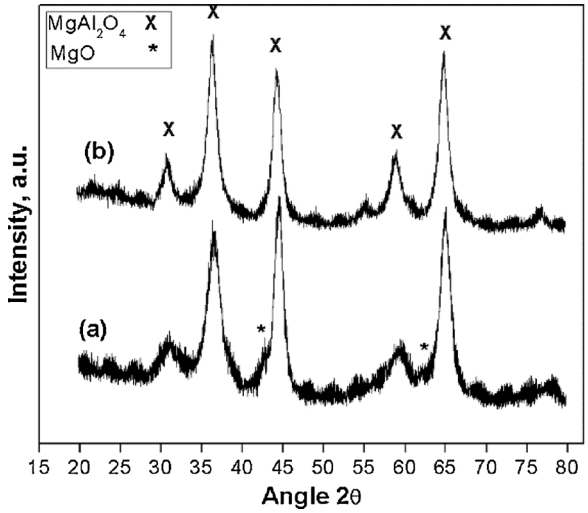

Fig. 3. Analysis by XRD of the layer materials of coated spheres obtained by BNAP method before purification step (a) and CN2 method (b).

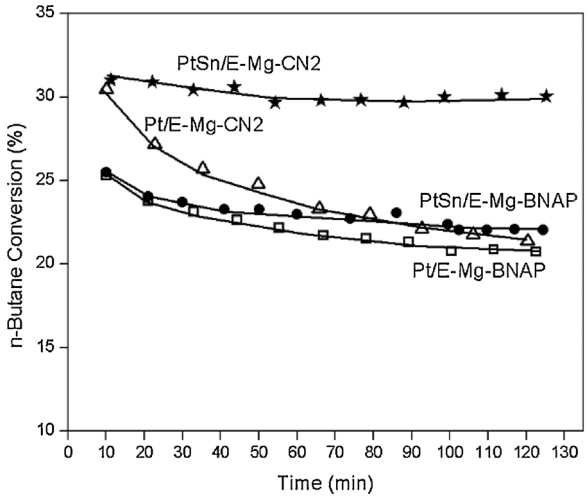

Fig. 4. Results of conversion of n-butane along the reaction time in n-butane dehydrogenation for Pt and PtSn catalysts.

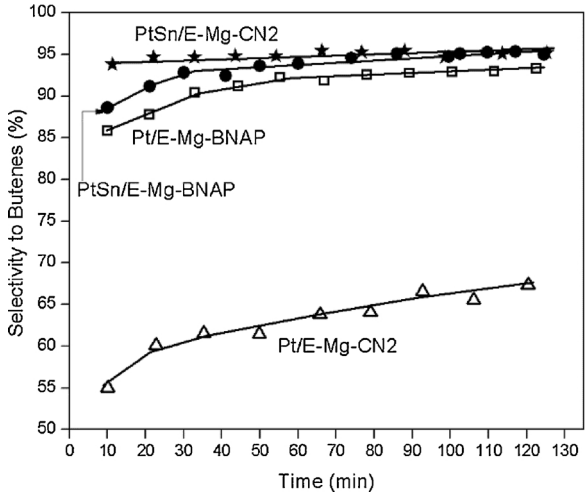

Fig. 5. Results of selectivity to butenes along the reaction time in n-butane dehydrogenation for Pt and PtSn catalysts.

chemisorption value with respect to Pt/E-Mg-CN2 catalyst, whereas the PtSn/E-Mg-BNAP catalyst showed a decrease of 1.3 times in the hydrogen chemisorption value with respect to the corresponding Pt catalyst. This behavior of the bimetallic catalysts with respect to the corresponding monometallic ones is also observed for the initial rates of CH dehydrogenation and CP hydrogenolysis (see Table 1). In this sense, it is important to highlight the pronounced decrease of the CP hydrogenolysis when Sn is added to Pt/E-Mg-CN2 catalyst, which is consistent with the increase in the selectivity to butenes of this bimetallic catalyst. Furthermore, the activation energy values in CH dehydrogenation (E_{CH}) are much higher for the PtSn/E-Mg-CN2 catalyst than for the Pt/E-Mg-CN2 one. For this structure-insensitive reaction, the activation energy can be modified if the nature of the metallic site is electronically changed by some effect, such as the influence of a second metal. This means that there is an important electronic modification of Sn on the Pt sites in the catalyst prepared by CN2 method. On the other hand, the decrease of the activation energy for the PtSn/E-Mg-BNAP sample with respect to the corresponding monometallic one could be due to geometric effects of the promoter on Pt. In conclusion, only geometric effects, such as dilution and blockage can be attributed to the Sn on the active sites of Pt in PtSn/E-Mg-BNAP catalyst. For the PtSn/E-Mg-CN2 catalyst, the promoter would be producing electronic effects (with probable alloys formation) on the Pt sites, in addition to geometric effects.

TPR profiles of Pt and PtSn catalysts supported on E-Mg-CN2 and E-Mg-BNAP are shown in Figs. 7 and 8. In agreement with results of test reactions and H_2 chemisorption (see Table 1), a higher interaction between Pt and Sn is observed in the PtSn/E-Mg-CN2 catalyst (Fig. 7c) in comparison to the PtSn/E-Mg-BNAP one (Fig. 8c). In the profile corresponding to the first bimetallic sample, there is an important increase of the reduction area of the main peak, whose maximum is placed at 259 °C, with respect to the corresponding monometallic catalyst (main peak placed at 254 °C, see Fig. 7b). This phenomenon is not observed in the PtSn/E-Mg-BNAP catalyst (Fig. 8c), in which the reduction area of the main peak (at 283 °C) is similar to the reduction area of the main peak of the Pt/E-Mg-BNAP catalyst, at 242 °C (Fig. 8b). These results would be evidencing a higher co-reduction effect of the active metal and the promoter in PtSn/E-Mg-CN2 catalyst and a probable PtSn alloy formation.

Figs. 9 and 10 show the XPS spectra of the Sn $3d_{5/2}$ signal corresponding to both bimetallic catalysts. From the deconvolution of both spectra, two peaks at 484.9 and 486.4 eV, and 485.4 and 486.7 eV for PtSn/E-Mg-BNAP (Fig. 9) and PtSn/E-Mg-CN2 (Fig. 10), respectively, were obtained. The first peak corresponds to zerovalent Sn, while the second one represents the oxidized Sn species [31]. For both catalysts, Sn is mainly found as Sn(II)/Sn(IV) species, while a lower proportion corresponds to Sn(0). The PtSn/E-Mg-CN2 catalyst has a higher percentage of Sn (0) (29%) than the PtSn/E-Mg-BNAP catalyst (25%). This difference is not significant, but it agrees with the higher interaction between Pt and Sn in the PtSn/E-Mg-CN2 catalyst. This effect is also evidenced with other characterization results, such as TPR and test reactions. In this sense, the PtSn alloy formation in the catalyst with the highest metallic interaction and promoter reducibility is more probable to occur. Regarding the reducibility of Pt, XPS results of the Pt 4f level for bimetallic PtSn catalysts indicate, in both cases, only the presence of zerovalent platinum. The doublets corresponding to $Pt4f_{7/2}$ and $Pt4f_{5/2}$ appeared at binding energies of 71.1–74.5 eV and 71.4–74.8 eV for PtSn/E-Mg-BNAP and PtSn/E-Mg-CN2 catalysts, respectively [31].

The distributions of metallic particle sizes obtained by TEM for mono and bimetallic catalysts supported on BNAP and CN2 are displayed in Figs. 11 and 12. Bimetallic catalysts showed slightly smaller average particle sizes, compared to the corresponding monometallic ones. Therefore, the decrease in the hydrogen chemisorption values of the bimetallic catalysts could not be caused by the increase of their metallic particle sizes. In this sense, the presence of geometric and/or electronic effects of the Sn on Pt sites would be responsible for this phenomenon, as explained above.

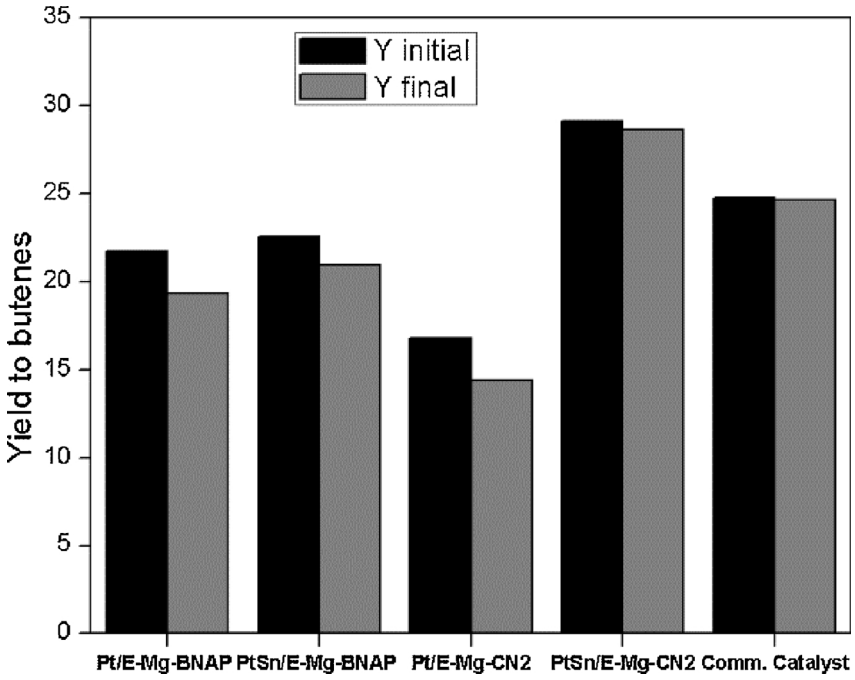

Fig. 6. Values of initial and final yields to butenes for Pt and PtSn catalysts in n-butane dehydrogenation reaction.

Table 1
Results of hydrogen chemisorption (H2), metallic dispersion (D), initial rate (R^{o}_{CP}) of cyclopentane hydrogenolysis, initial rate (R^{o}_{CH}) and activation energy (ECH) of cyclohexane dehydrogenation.

CATALYST	H_2 (μmol H_2 g cat^{-1})	D (%)	R^{o}_{CH} (mol CH g^{-1} h^{-1})	E_{CH} (Kcal mol^{-1})	R^{o}_{CP} (mol CP g^{-1} h^{-1})
Pt/E-Mg-BNAP	3.47	45	18.63	27.66	1.96
PtSn/E-Mg-BNAP	2.71	–	4.74	14.32	1.04
Pt/E-Mg-CN2	6.76	88	26.31	17.70	2.81
PtSn/E-Mg-CN2	0.88	–	2.47	31.28	0.79

By comparing the influence of the coating methods, used for the synthesis of catalytic supports, on the size of the metallic particles, it is observed that the catalysts prepared by the CN2 method have smaller sizes than the catalysts prepared by BNAP. What is more, the PtSn/E-Mg-CN2 catalyst has the lowest average particle size, 1.2 nm, and 98% of their metallic particles have a size smaller than 1.5 nm (Fig. 12).

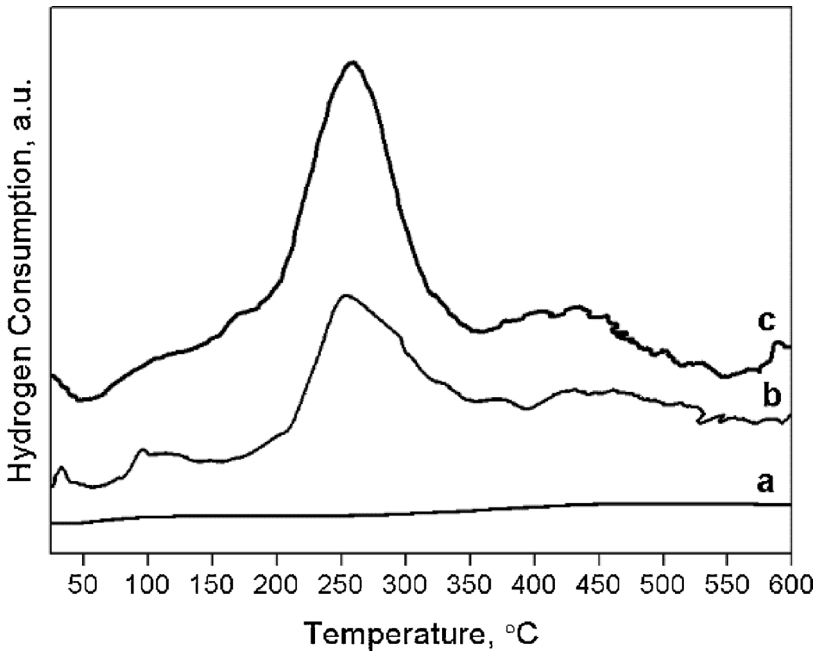

Fig. 7. TPR profiles of the Sn (a), Pt (b) and PtSn (c) catalysts supported on spheres coated by CN2 method.

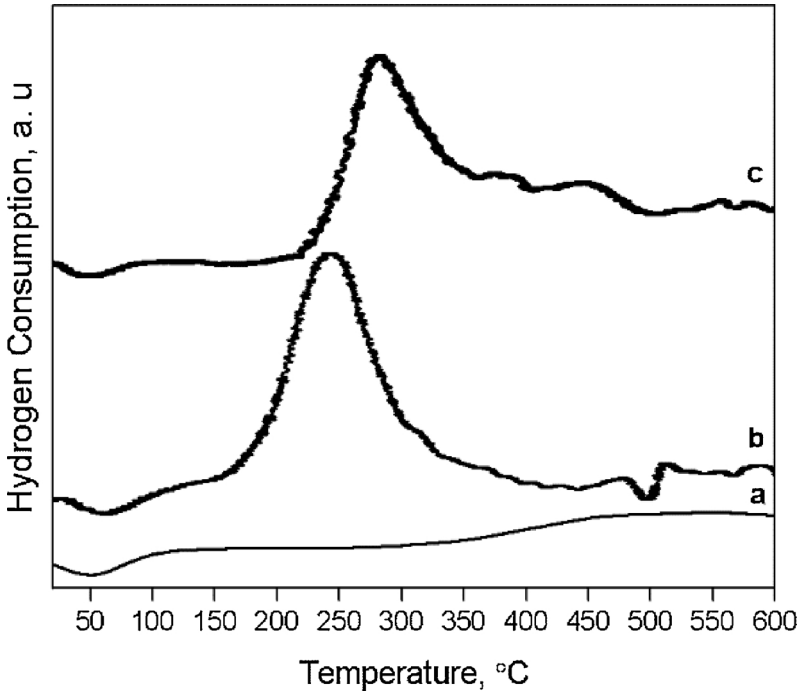

Fig. 8. TPR profiles of the Sn (a), Pt (b) and PtSn (c) catalysts supported on spheres coated by BNAP method.

These results agree with those of hydrogen chemisorption, where the catalysts prepared by CN2 method showed higher hydrogen chemisorption values than the catalysts synthesized by BNAP one. However, for bimetallic catalysts, the presence of electronic and geometric effects distorts chemisorption measurements, and hence it makes difficult to correlate them with the size of metallic particles. TEM images of mono and bimetallic catalysts are shown in Figures 1S, 2S, 3S and 4S.

Considering results of both n-butane dehydrogenation reaction and catalytic characterization, the promoter role of Sn on Pt strongly decreases the hydrogenolytic capacity of the active metal by geometric and electronic effects, improving the selectivity to butenes. Besides, it also decreases the deactivation and therefore increases the catalyst stability. With respect to the activity of mono and bimetallic catalysts, the first n-butane conversion point obtained in the flow experiments (at 10 min of the reaction time) corresponds to the reaction of n-butane on a modified surface in which hydrogenolytic sites were deactivated. From previous results of pulse experiments with n-butane [32], the activity of monometallic catalysts was higher than that of bimetallic ones at the first stages of the reaction, but the deactivation was more pronounced for monometallic samples. In consequence, it can be expected a higher initial activity of bimetallic catalysts than monometallic ones at 10 min of the reaction time in flow experiments.

By analyzing the catalytic activity per active metal site, the identification of these sites by hydrogen chemisorption is not clear. In this sense the choice of the concentration of surface metal sites as those measured by TEM seems more appropriate. The metallic dispersion (D)

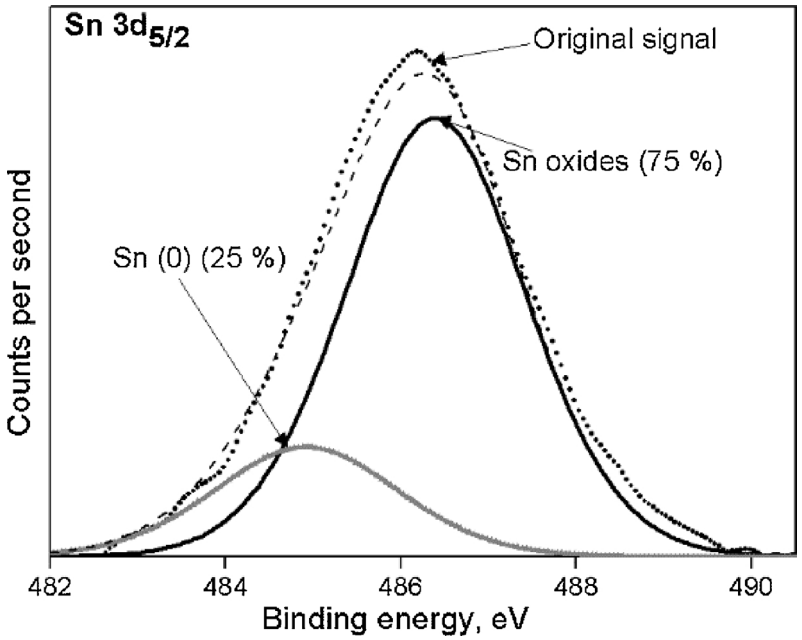

Fig. 9. XPS spectrum of the Sn 3d5/2 signal for PtSn catalyst supported on spheres coated by BNAP method.

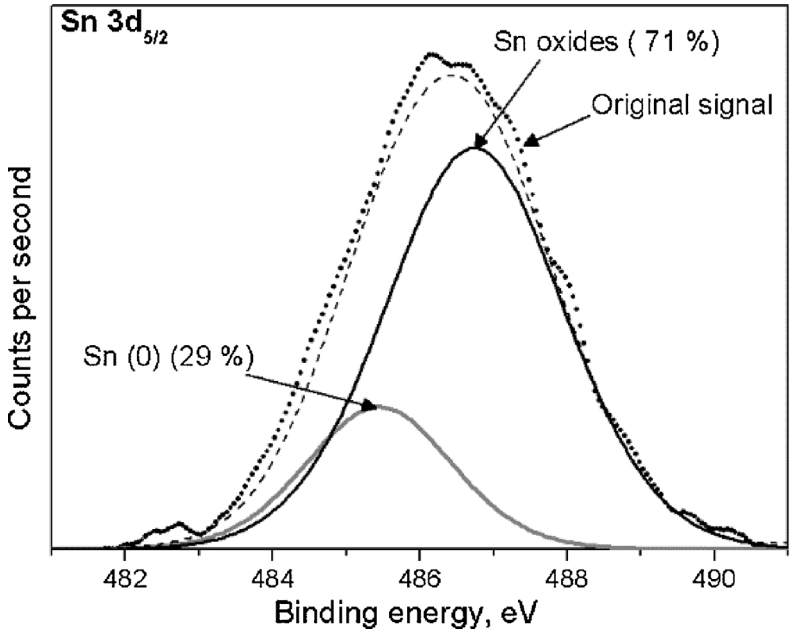

Fig. 10. XPS spectrum of the Sn 3d5/2 signal for PtSn catalysts supported on spheres coated by CN2 method.

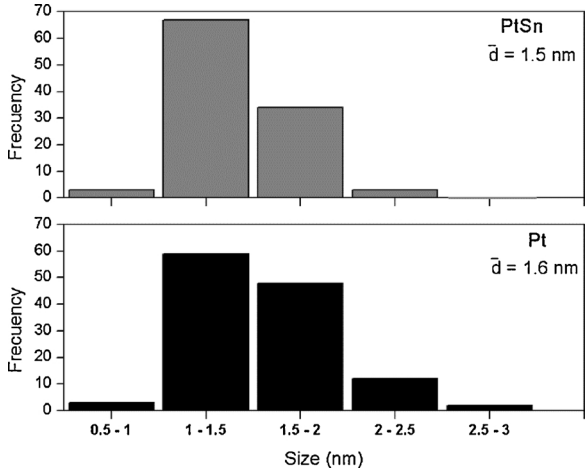

Fig. 11. Distribution of metallic particle sizes obtained by TEM for Pt and PtSn catalysts supported on spheres coated by BNAP method.

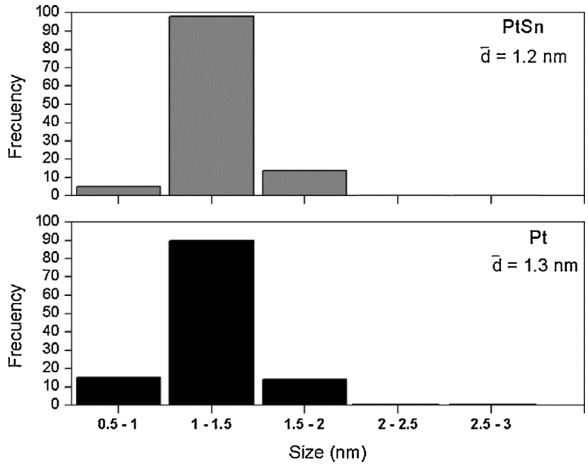

Fig. 12. Distribution of metallic particle sizes obtained by TEM for Pt and PtSn catalysts supported on spheres coated by CN2 method.

was estimated by using the expression D = 1.13/d, where d is the average particle size in nm. This equation was deduced assuming that all metal particles were spherically shaped [33]. When the TEM based TOF values were calculated, it was found that initial TOF values were similar for all samples, between 0.73 and 0.78 s^{-1}. But at 120 min time-on-stream, PtSn/E-Mg-CN2 sample (the catalyst with the best catalytic performance) had a TOF value of 0.71 s^{-1}, higher than the TOF of Pt/E-Mg-CN2 (0.54 s^{-1}), Pt/E-Mg-BNAP (0.66 s^{-1}) and PtSn/E-Mg-BNAP (0.65 s^{-1}). It must be stressed that PtSn/E-Mg-CN2 sample not only had the highest final TOF value but also the highest dispersion and the highest activity per unit catalyst mass. As the bulk catalyst density is the same for all samples, for practical purposes PtSn/E-Mg-CN2 catalyst has the highest activity per unit reactor volume.

4. Conclusions

It is possible to conclude that the developed coating methods achieve a stable, porous and uniform $MgAl_2O_4$ layer on the spherical nucleus, which has a good interaction with the metals leading to very high metallic dispersions.

The main effects of Sn in bimetallic catalysts were the improvement of the selectivity to butenes and the decrease of the catalytic deactivation. The use of an inert structured support and the Sn addition to Pt produce the following effects: i) Inhibition of the breaking of C—C bonds which give light alkanes (C_1, C_2 and C_3 products), ii) inhibition of the formation of diolefins that lead to coke precursors. This phenomenon is caused by an increase of the electronic density of the Pt atoms (by the Sn promotion) which would allow a rapid desorption of monoolefins. These effects were more pronounced in the PtSn/E-Mg-CN2 catalyst, which showed high n-butane conversion, very low deactivation and high selectivity to butenes along the reaction time. Moreover this catalyst displayed higher yields to butenes than a commercial structured multimetallic catalyst. In agreement with these results of the dehydrogenation reaction, the PtSn/E-Mg-CN2 catalyst showed high interaction between Pt and Sn with probable alloy formation and the lowest metallic particle size of all the studied catalysts.

Acknowledgements

Authors thank the Universidad Nacional del Litoral (CAI+D

Program) and CONICET (PIP 0075) from Argentina, for the financial support of this research, and G. M. Baez for the experimental assistance.

Appendix A. Supplementary data

Supplementary material related to this article can be found, in the online version, at doi: https://doi.org/10.1016/j.apcata.2018.09.005.

References

[1] S.A. Bocanegra, A.A. Castro, A. Guerrero-Ruíz, O.A. Scelza, S.R. de Miguel, Chem. Eng. J. 118 (2006) 161–166.
[2] K. Xia, W.-Z. Lang, P.-P. Li, L.-L. Long, X. Yan, Y.-J. Guo, Chem. Eng. J. 284 (2016) 1068–1079.
[3] S.A. Bocanegra, P.D. Zgolicz, O.A. Scelza, S.R. de Miguel, Catal. Commun. 10 (2009) 1463–1466.
[4] N. Homs, J. Llorca, M. Riera, J. Jolis, J.L.G. Fierro, J. Sales, P. Ramírez de la Piscina, J. Mol. Catal. A: Chem. 200 (2003) 251–259.
[5] S.A. Bocanegra, S.R. de Miguel, I. Borbath, J.L. Margitfalvi, O.A. Scelza, J. Mol. Catal. A: Chem. 301 (2009) 52–60.
[6] Y. Zhang, Y. Zhou, J. Shi, S. Zhou, Z. Zhang, S. Zhang, M. Guo, Fuel Process. Technol. 111 (2013) 94–104.
[7] S.A. Bocanegra, A. Guerrero-Ruiz, O.A. Scelza, S.R. de Miguel, Catal. Industry 5 (1) (2013) 61–73.
[8] A.D. Ballarini, S.R. de Miguel, A.A. Castro, O.A. Scelza, Appl. Catal. A 467 (2013) 235–245.
[9] S. Furukawa, A. Tamura, K. Ozawa, T. Komatsu, Appl. Catal. A 469 (2014) 300–305.
[10] E.L. Jablonski, A.A. Castro, Scelza O.A, S.R. de Miguel, Appl. Catal. A 183 (1) (1999) 189–198.
[11] H. Armendáriz, A. Guzmán, J. Toledo, M. Llanos, A. Vazquez, G. Aguilar-Ríos, Appl. Catal. A 211 (2001) 69–80.
[12] S. Bocanegra, S.R. de Miguel, A.A. Castro, O.A. Scelza, Catal. Lett. 96 (3-4) (2004) 129–140.
[13] Y.-L. Shan, T. Wang, Z.-J. Sui, Y.-A. Zhu, X.-G. Zhou, Catal. Commun. 84 (2016) 85–88.
[14] V. Meille, Appl. Catal. A 315 (2006) 1–17.
[15] C.G. Visconti, E. Tronconi, L. Lietti, G. Groppi, P. Forzatti, C. Cristiani, R. Zennaro, S. Rossini, Appl. Catal. A 370 (2009) 93–101.
[16] C. Cristiani, C.G. Visconti, S. Latorrata, E. Bianchi, E. Tronconi, G. Groppi, P. Pollesel, Stud. Surf. Sci. Catal. 175 (2010) 653–656.
[17] Y. Kim, H. Lee, T. Lim, H.-J. Kim, O. Kwon, J. Power Sources 364 (2017) 16–22.
[18] Y. Zhou, H. Zhang, Y. Yan, J. Taiwan. Inst. Chem. Eng. 84 (2018) 162–172.
[19] M.-Y. Kim, J.-S. Choi, T.J. Toops, E.-S. Jeong, S.-W. Han, V. Schwartz, J. Chen, Catalysts 3 (1) (2013) 88–103.
[20] G. Chen, S. Li, Q. Yuan, Catal. Today 120 (2007) 63–70.
[21] M. Karches, M. Morstein, P.R. Von Rohr, R.L. Pozzo, J. Giombi, M.A. Baltanas, Catal. Today 72 (3-4) (2002) 267–279.
[22] Y. Wang, F. Zhang, S. Xu, L. Yang, D. Li, D.G. Evans, X. Duan, Chem. Eng. Sci. 63 (2008) 4306–4312.
[23] A.D. Ballarini, P. Zgolicz, I.M.J. Vilella, S.R. de Miguel, A.A. Castro, O.A. Scelza, Appl. Catal. A 381 (2010) 83–91.
[24] D. Browne, H. Li, E. Giorgi, S. Dutta, J. Biser, R.P. Vinci, H.M. Chan, J. Mater. Sci. 44 (2009) 1180–1186.
[25] A. Saberi, F. Golestani-Fard, H. Sarpoolaky, M. Willert-Porada, T. Gerdes, R. Simon, C. Liebscher, Ceram. Int. 35 (2009) 457–461.
[26] C. Zhang, J. Zhang, J. Ma, Int. J. Hydrogen Energy 37 (2012) 12941–12946.
[27] S.A. Bocanegra, A.D. Ballarini, O.A. Scelza, S.R. de Miguel, Mater. Chem. Phys. 111 (2008) 534–541.
[28] S.A. Bocanegra, A.D. Ballarini, O.A. Scelza, S.R. de Miguel, Proc. Mater. Sci. 9 (2015) 69–78.
[29] G.M. Baez, O.A. Scelza, S.R. de Miguel, S.A. Bocanegra, Mater. Res. 18 (2) (2015) 404–410.
[30] D.W. Blakely, G.A. Somorjai, J. Catal. 42 (1976) 181–196.
[31] J.F. Moulder, W.F. Stickle, P.E. Sobol, K.D. Bomben, Handbook of X-Ray Photoelectron Spectroscopy, Jill Chastain, Minnesota, 1992.
[32] S.A. Bocanegra, A. Guerrero-Ruiz, S.R. de Miguel, O.A. Scelza, Appl. Catal. A 277 (2004) 11–22.
[33] M. Aramendía, V. Borau, C. Jiménez, J.M. Marinas, A. Moreno, Eng. Asp. 106 (1996) 161–165.